

Water-soluble dendritic-linear triblock copolymer-modified magnetic nanoparticles: preparation, characterization and drug release properties†Xiaomeng Wu,^a Xiaohua He,^{*ab} Liang Zhong,^a Shaoliang Lin,^b Dali Wang,^c Xinyuan Zhu^{*c} and Deyue Yan^{ac}

Received 15th April 2011, Accepted 16th June 2011

DOI: 10.1039/c1jm11613d

One route has been employed to prepare dendritic-linear block copolymer modified superparamagnetic iron oxide nanoparticles (SPIONs), which consist of a Fe₃O₄ magnetic nanoparticle core and a dendritic-linear block copolymer, the focal point polyamidoamine-type dendron-*b*-poly(2-dimethylaminoethyl methacrylate)-*b*-poly(*N*-isopropylacrylamide) (PAMAM-*b*-PDMAEMA-*b*-PNIPAM) shell by two-step atom transfer radical polymerization (ATRP). Firstly, Fe₃O₄ nanoparticles were prepared by a high-temperature solution phase reaction in the presence of iron(III) acetylacetonate [Fe(acac)₃], oleic acid and oleylamine. Then propargyl focal point PAMAM-type dendron (generation 2.0, denoted as propargyl-D_{2.0}) with four carboxyl acid end groups as a cap displaced the oleic acid and oleylamine on the surfaces. Subsequently, an initiator for ATRP was introduced onto the propargyl-D_{2.0}-modified Fe₃O₄ nanoparticle surfaces *via* click chemistry with 2'-azidoethyl-2-bromoisobutylate (AEBIB). PDMAEMA and PNIPAM were grown gradually from nanoparticle surfaces using two-step copper-mediated ATRP. Finally, a crosslinking reaction between PDMAEMA block with 1,2-bis(2-iodoethoxy)ethane (BIEE) was used to stabilize the nanoparticles and reverse aggregation. The modified nanoparticles were subjected to detailed characterization using FT-IR, DLS, XRD and TGA. Magnetization measurements confirmed the characteristic superparamagnetic behavior of all magnetic nanoparticles under room temperature. In addition, doxorubicin (DOX) as an anticancer drug model was loaded into the dendritic-linear block copolymer shell of the modified nanoparticles, and subsequently the drug release was performed in phosphoric acid buffer solution (pH 7.4) at 25 °C or 37 °C. The results verify that dendritic-linear block copolymer-modified nanoparticles as a drug carrier possess thermosensitive drug release behaviors. Furthermore, a methyl tetrazolium (MTT) assay of DOX-loaded dendritic-linear block copolymer-modified nanoparticles against Hela cells was evaluated. The results show that the modified nanoparticles can be used for drug delivery.

^aDepartment of Chemistry, East China Normal University, 3663 Zhongshan North Road, Shanghai, 200062, China. E-mail: xhhe@chem.ecnu.edu.cn

^bThe Key Laboratory of Advanced Polymer Materials of Shanghai, School of Materials Science and Engineering, East China University of Science and Technology, Shanghai, 200237, China

^cSchool of Chemistry & Chemical Engineering, Shanghai Jiao Tong University, 800 Dongchuan Road, Shanghai, 200240, China. E-mail: xyzhu@sjtu.edu.cn

† Electronic supplementary information (ESI) available: Experimental procedures for the synthesis and characterization of 2'-azidoethyl 2-bromoisobutylate (AEBIB) and propargyl focal point PAMAM-type dendrons with four carboxyl acid end groups (generation 2.0, denoted as propargyl-D_{2.0}-COOH), the procedure for obtaining functional block copolymers from the modified magnetic nanoparticles, the graft density of the modified Fe₃O₄ nanoparticles and the stability of Fe₃O₄ nanoparticles. See DOI: 10.1039/c1jm11613d

Introduction

Over the past decade, magnetic nanoparticles (MNPs) have been intensively pursued not only for their fundamental scientific interest but also for rich technological applications.^{1–8} Among them, biological applications have developed dramatically for magnetic resonance imaging (MRI),^{7–12} bacterial detection,⁹ hyperthermia,^{6,13} protein purification,⁹ cell separation⁶ and drug delivery^{6,9,14} *etc.* Among the wide variety of magnetic nanoparticles, iron oxide nanoparticles (usually Fe₃O₄ and Fe₂O₃) have certainly been and still are the most intensively investigated. This is due to their remarkable magnetic properties and low toxicity. To date, several synthetic methods have been applied to prepare magnetic iron oxide nanoparticles, including co-precipitation of iron(II) and iron(III) ions in basic solution,^{15–18} an emulsion method using pre-synthesized magnetite stabilized with oleic acid,¹⁹ organic solution-phase decomposition of the iron precursor at high temperature^{10,20–23} *etc.* In these methods, the

organic solution-phase decomposition of the iron precursor at high temperature has been proved to be effective in the preparation of magnetic nanoparticles with good crystallinity, and a relatively monodisperse and controlled size distribution.

In practical biological applications, magnetic iron oxide nanoparticles are required to either disperse in water easily or be superparamagnetic,¹ which can be helpful to improve the stability in the internal environment of the human body. Generally, there are two kinds of strategies to enhance the stability and biocompatibility of the magnetic iron oxide nanoparticles. The first strategy is to control the particle size to obtain the superparamagnetism by using suitable synthetic methods, such as organic solution-phase decomposition of the iron precursor at high temperature.²² Superparamagnetic iron oxide nanoparticles (SPIONs) do not retain any magnetism after removal of the magnetic field and can prevent magnetic aggregation after exposure to a magnetic field.²⁴ The second one is to modify the particle surface to enhance the biocompatibility and stability. Up to now, some surface-modified methods have been achieved with the help of monomeric stabilizers,^{25,26} inorganic stabilizers^{27–29} or polymer stabilizers.^{10,11,15–18,20,21,30–39} It must be pointed out that the latter not only provides stability to the corresponding magnetic nanoparticles but also allows further biological derivatization. Usually, two different approaches can be adopted to modify nanoparticles with polymers: “grafting onto” and “grafting from” the nanoparticle surface. The “grafting onto” method involves the as-synthesized polymers being grafted onto the nanoparticle surface by electrostatic, hydrophobic interactions or through the affinity of certain chemical groups.^{17,33,38,40} However, grafting the as-synthesized polymer chains onto a single small particle surface may be more difficult, since polymer chains can bind more than a particle at the same time, and then forming polymer-coated nanoparticle clusters.³³ On the contrary, the “grafting from” method, a surface-initiated polymerization method, can be more suitable to modify the small particle surfaces and prevent the occurrence of nanoparticle clusters because the coating polymers are grown directly from the nanoparticle surface. At present, many polymer-coated magnetic iron oxide nanoparticles have been achieved by the “grafting from” method using different polymerization processes, such as atom transfer radical polymerization (ATRP),^{6,20,19,31,34} ring-opening polymerization (ROP),^{20,41} *etc.* Especially mentioned, ATRP is a controlled/living polymerization process which can produce polymer chains with controllable lengths and for which a broad variety of monomers can be used.⁴² So, either the thickness of the polymer shell or the properties of polymer-coated nanoparticles can be easily tuned. Up to now, ATRP has been widely used for nanoparticle surface-initiated modification.⁴³

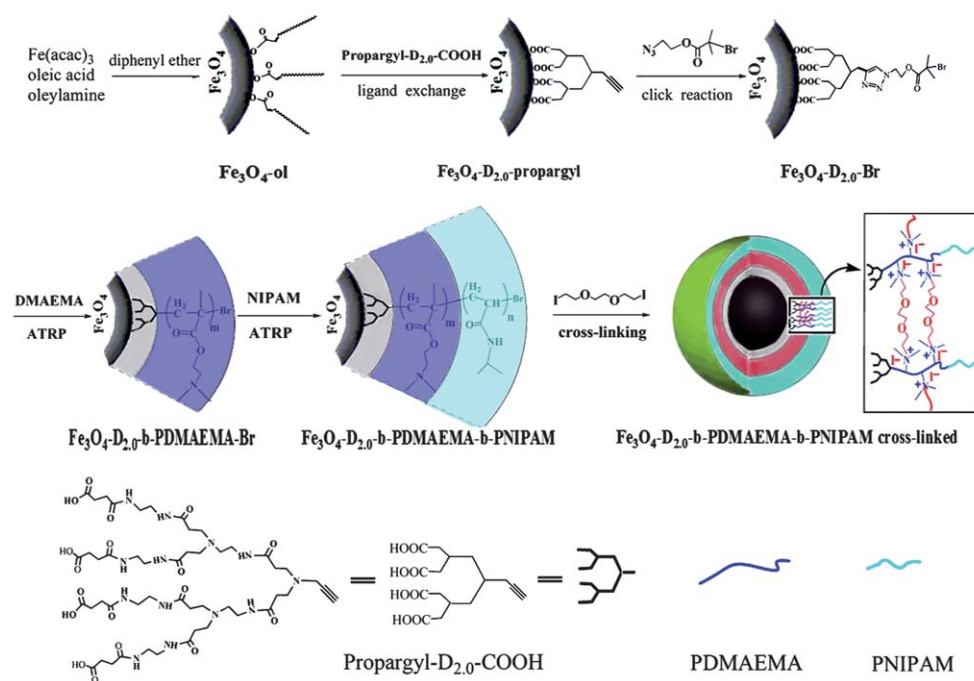
In this report, dendritic-linear block copolymer-modified magnetic iron oxide nanoparticles were designed and prepared by the combination of the “grafting to” and “grafting from” approach. Firstly, magnetic iron oxide nanoparticles were prepared by the method of the organic solution-phase decomposition of the iron precursor at high temperature. Second, the propargyl focal point polyamidoamine (PAMAM)-type dendron, bearing four carboxyl acid end groups, can cap on magnetic iron oxide nanoparticle surfaces to stabilize the nanoparticles by means of a “grafting onto” approach. The surface-

initiator was introduced onto the propargyl group by a click reaction. Then, using two-step surface-initiated ATRP, poly(2-dimethylaminoethyl methacrylate) (PDMAEMA) chains and poly(*N*-isopropylacrylamide) (PNIPAM) chains were sequentially introduced onto the magnetic nanoparticle surfaces by means of a “grafting from” approach. PAMAM-*b*-PDMAEMA-*b*-PNIPAM block copolymer-modified magnetic iron oxide nanoparticles were successfully achieved. Moreover, cross-linking reactions within the PDMAEMA chains were carried out to further stabilize the magnetic iron oxide nanoparticles. Our synthesis protocol possesses the following merits: (1) further enhancing the stability of SPIONs. Dendritic polymers are relatively novel polymers with many functional groups on the surface, perfect chemical structures, internal cavities and nano-size *etc.*, which provide dendritic polymers with many potential biomedical applications.^{44,45} The as-synthesized focal point PAMAM-typed dendron bearing four carboxyl acid end groups was chelated to SPION surfaces like a cap, which was beneficial to further stabilize SPIONs. On the other hand, the stability of polymer-modified nanoparticles can be also increased by cross-linking.⁴⁶ Cross-linking reactions within PDMAEMA chains can be helpful to stabilize magnetic iron oxide nanoparticles. (2) Offering more internal cavities due to PAMAM-type dendron coating can improve the encapsulation efficiency of functional molecules (such as drugs) into the polymer-modified shell layer of SPIONs. (3) PNIPAM possesses temperature sensitivity and biocompatibility, which has been widely applied in the biomedical area.⁴⁷ SPIONs coated with PNIPAM chains can not only prevent the agglomeration but also increase biocompatibility. To expand the biomedical applications of SPIONs, doxorubicin (DOX), as an anticancer drug model, can be loaded into the as-synthesized nanoparticle system and the drug release behaviors at different temperatures were investigated. At the same time, the cytotoxicity of the DOX-loaded nanoparticle system was also evaluated. To the best of our knowledge, there have been few reports concerning the synthesis of dendritic-linear block copolymer-modified magnetic nanoparticles. The synthesis and surface modification of SPIONs is illustrated schematically in Scheme 1.

Experimental section

Materials

Iron(III) acetylacetonate (Fe(acac)₃, 98%), oleic acid (OA, 90%) and oleylamine (OAm, 80%) were purchased from Aladdin-Reagent (Shanghai) Ltd. 2-Dimethylaminoethyl methacrylate (DMAEMA, 99%), 1,1,4,7,7-pentamethyldiethylenetriamine (PMDETA, 99%), 2,2'-bipyridine (bpy, 99%), *N*-isopropylacrylamide (NIPAM, 99.8%) and 3-(4,5-dimethyl-thiazol-2-yl)-2,5-diphenyltetrazolium bromide (MTT) were purchased from Aldrich. CuBr and CuCl (Shanghai Chemical Reagent Co., A.R. grade) were purified by stirring in glacial acetic acid overnight, filtered, washed with ethanol and then dried in a vacuum oven at 60 °C overnight. Phenyl ether (99.9%), *N,N*-dimethylformamide (DMF, A.R. grade) and dimethyl sulfoxide (DMSO) were purchased from Shanghai Chemical Reagent Company and dried over calcium hydride (CaH₂) and distilled under reduced pressure. 1,2-bis(2-iodoethoxy)ethane (BIEE) was



Scheme 1 The synthesis and surface modification of superparamagnetic Fe_3O_4 nanoparticles.

synthesized according to the published procedure.⁴⁸ 2'-Azidoethyl 2-bromoisobutylate (AEBIB) and propargyl focal point PAMAM-type dendrons with four carboxylic acid end groups (generation 2.0, denoted as propargyl- $\text{D}_{2.0}$ -COOH) were synthesized according to the ESI†. Tris(2-(dimethylamino)ethyl)amine (Me_6TREN) was synthesized according to the literature procedures.⁴⁹ Doxorubicin hydrochloride (DOX-HCl) was purchased from Zhejiang Hisun Pharmaceutical Co., Ltd. Other chemical reagents were purchased from Shanghai Chemical Reagent Company and purified by conventional procedures if needed.

Synthesis of oleic acid-coated magnetic iron oxide nanoparticles ($\text{Fe}_3\text{O}_4\text{-ol}$)

Magnetic nanoparticles were prepared according to the similar procedure reported by Lattuada *et al.*²⁰ The procedure was as follows: $\text{Fe}(\text{acac})_3$ (5.7 g, 16 mmol), OA (13.6 g, 48 mmol), OAm (12.8 g, 48 mmol) and phenyl ether (120 mL) were mixed in a four-necked round bottom flask and stirred vigorously under a constant flow of nitrogen. The mixture was heated to 100 °C for 40 min and then heated to 200 °C for 2 h under nitrogen. Sequentially, the mixture was heated to reflux (~265 °C) for another 1 h under a blanket of nitrogen. The dark-brown mixture was cooled to room temperature under nitrogen. Ethanol (~200 mL) was added to the mixture and the black precipitates were collected *via* centrifugation. The black precipitates were dissolved in hexane and purified by centrifugation for removal of any residue. The black products were dried in a vacuum oven at room temperature.

Synthesis of propargyl- $\text{D}_{2.0}$ -COOH-coated magnetic iron oxide nanoparticles ($\text{Fe}_3\text{O}_4\text{-D}_{2.0}$ -propargyl)

$\text{Fe}_3\text{O}_4\text{-ol}$ (0.8 g) prepared as described above was dispersed in 40 mL of a mixture of anhydrous solvent containing 1,2-

dichlorobenzene, DMF and methanol (volume ratio 2 : 2 : 1), and sonicated for 10 min, to which the solution of 1.22 g of propargyl- $\text{D}_{2.0}$ -COOH dissolved in dried methanol (10 mL) was added. The mixture was then mechanically stirred at 65 °C under nitrogen for 48 h. After cooling to room temperature, an excess of methanol was added to the mixture, and the black particles were magnetically precipitated and subsequently separated by centrifugation. The nanoparticles were washed with methanol to remove propargyl- $\text{D}_{2.0}$ -COOH residues and dried in a vacuum oven at room temperature.

Synthesis of magnetic nanoparticle macroinitiators ($\text{Fe}_3\text{O}_4\text{-D}_{2.0}\text{-Br}$)

$\text{Fe}_3\text{O}_4\text{-D}_{2.0}$ -propargyl (0.15 g) was dispersed in DMF (8 mL), to which AEBIB (0.4 g, 1.7 mmol) was added. The mixture was purged with pure nitrogen for 30 min, CuBr (26.5 mg, 0.18 mmol) and PMDETA (38.0 mg, 0.18 mmol) were then added. Under the protection of nitrogen, the mixture was mechanically stirred for 24 h at 45 °C. After cooling to room temperature, 30 mL of diethyl ether was added to the mixture, and the black particles were magnetically precipitated and subsequently separated by centrifugation. The nanoparticles were washed with methanol to remove any residues and dried in a vacuum oven at room temperature.

Synthesis of PDMAEMA-modified magnetic iron oxide nanoparticles ($\text{Fe}_3\text{O}_4\text{-D}_{2.0}\text{-b-PDMAEMA-Br}$)

$\text{Fe}_3\text{O}_4\text{-D}_{2.0}\text{-Br}$ (0.15 g), methanol (4 mL) and DMAEMA (3.0 g, 19.1 mmol) were charged into a reaction tube. After purging with pure nitrogen for 30 min, CuBr (89.0 mg, 0.6 mmol) and bpy (100 mg, 0.6 mmol) were added into the mixture under the protection of nitrogen. The mixture was stirred for 24 h at room

temperature under nitrogen atmosphere. Then, an excess of diethyl ether was added to the mixture, and the black particles were magnetically precipitated and subsequently separated by centrifugation. The nanoparticles were purified from methanol to diethyl ether three times and dried in a vacuum oven at room temperature.

Synthesis of PDMAEMA-*b*-PNIPAM block copolymer-modified magnetic iron oxide nanoparticles (Fe₃O₄-D_{2.0}-*b*-PDMAEMA-*b*-PNIPAM)

Fe₃O₄-D_{2.0}-*b*-PDMAEMA-Br (0.15 g), NIPAM (0.7 g, 6.2 mmol), Me₆TREN (23 mg, 0.1 mmol) and 2-propanol (4 mL) were charged into a reaction tube. After purging with pure nitrogen for 30 min, CuCl (10 mg, 0.1 mmol) was introduced into the mixture under the protection of nitrogen flow. After polymerization at room temperature under nitrogen for 24 h, the mixture was exposed to air and 30 mL of diethyl ether was added. The black particles were magnetically precipitated and subsequently separated by centrifugation. The nanoparticles were purified from 2-propanol to diethyl ether three times and dried in a vacuum oven at room temperature.

Cross-linking of Fe₃O₄-D_{2.0}-*b*-PDMAEMA-*b*-PNIPAM nanoparticles

Fe₃O₄-D_{2.0}-*b*-PDMAEMA-*b*-PNIPAM (0.15 g) prepared as described above was dissolved in ethanol (4 mL) and BIEE (0.2 g, 0.54 mmol) was then introduced into the mixture. The [BIEE]/[DMAEMA] molar ratio was fixed at 1 : 2, targeting a 100% degree of cross-linking. After stirring at room temperature under nitrogen for 48 h, the black particles were magnetically precipitated and subsequently separated by centrifugation. The black nanoparticles were further washed using diethyl ether for removal of any residues and dried in a vacuum oven at room temperature.

Loading block copolymer-modified nanoparticles with DOX and *in vitro* drug release

DOX-HCl (3.0 mg) was dissolved in methanol (6 mL), and triethylamine (0.05 mL) was then added into the solution to remove hydrochloride. The DOX solution was added dropwise with stirring to 3 mL of Fe₃O₄-D_{2.0}-*b*-PDMAEMA-*b*-PNIPAM nanoparticles (or Fe₃O₄-D_{2.0}-*b*-PDMAEMA-*b*-PNIPAM cross-linked nanoparticles) in methanol (concentration of 2.5 mg mL⁻¹). The mixture was shaken for 24 h in the dark at room temperature to allow the drug partition into the polymer shell. The black particles were magnetically precipitated and subsequently separated by centrifugation. The supernatant was also collected. The drug-loaded nanoparticles collected were further washed three times using methanol to remove completely the free DOX. All supernatant were gathered together to obtain the amount of free DOX. The drug loading efficiency was calculated as follows:

$$\text{Loading efficiency (\%)} = 100 \times \frac{(\text{initial amount of DOX} - \text{amount of free DOX})}{\text{initial amount of DOX}}$$

The drug-loaded nanoparticles quantified were immersed into the quantitative volume of phosphate-buffered solution (PBS) (0.01 M) with pH = 7.4 at 25 °C or 37 °C. After shaking for the

selected time intervals (5 h or 24 h) in the dark, the nanoparticles were recovered by magnetic separation and centrifugation. The supernatant was further diluted with methanol to constant volume and then monitored by a UV-vis spectrometer at 485 nm to determine the rate of drug release. The DOX concentration was determined according to the standard curves of DOX solution. Cumulative release was expressed as the total percentage of drug release and calculated from the following relationship:

$$\text{Cumulative release (\%)} = 100 \times W_t/W$$

where W_t was the weight of drug released from block copolymer-modified nanoparticles at time t and W was the total weight of drug loaded into the block copolymer-modified nanoparticles.

Cell culture and cell viability assay

Hela cells (human cervix carcinoma cell line) were cultured in Dulbecco's modified Eagle's medium (DMEM) supplied with 10% FBS (fetal bovine serum) and antibiotics (50 units mL⁻¹ penicillin and 50 units mL⁻¹ streptomycin) at 37 °C in a humidified atmosphere containing 5% CO₂ atmosphere.

Hela cells were chosen to assess the anticancer activity of the released DOX from DOX-loaded iron oxide magnetic nanoparticles as described above. Briefly, a series of solutions of DOX-loaded iron oxide magnetic nanoparticles were prepared in DMEM media, in which the final concentration of DOX ranged from 0.1 to 2 μg mL⁻¹. Hela cells with approximately 8000 cells well⁻¹ were seeded in 96-well plates in 200 μL medium for incubating for 24 h at 37 °C. Then, the culture medium was removed and replaced with 200 μL of fresh medium containing serial concentrations of DOX-loaded iron oxide magnetic nanoparticles to incubate the cells. After 24 h of incubation at 37 °C, 20 μL of 5 mg mL⁻¹ MTT assays stock solution in PBS was added to each well and the cells were incubated for another 4 h at 37 °C. Then, the medium containing unreacted dye was removed carefully and 200 μL DMSO per well was added to dissolve the obtained blue formazan crystals. The absorbance was measured in a BioTek Elx800 at a wavelength of 490 nm. To compare with the anticancer activity of the released DOX from DOX-loaded iron oxide magnetic nanoparticles, the same concentration of the free DOX was also assayed.

Characterization

Fourier transform infrared (FT-IR) spectra were recorded on a Perkin-Elmer Spectrum One spectrometer at frequencies ranging from 400 to 4000 cm⁻¹. Samples were thoroughly mixed with KBr and pressed into pellet form.

Transmission electron microscopy (TEM) analysis of iron oxide magnetic nanoparticles was performed on a JEOL 2100CX (200 kV) microscope. Drops of the solution of iron oxide magnetic nanoparticles were deposited and dried at room temperature on a carbon-coated copper grid.

Dynamic light scattering (DLS) measurements were performed with a Malvern Instruments particle sizer (HPPS-ET 5002, Malvern Instruments, UK) equipped with a He-Ne laser ($\lambda = 632.8$ nm). Scattered light was collected at a fixed angle of 173° for the duration of 5 min. All data were averaged over three measurements.

Wide-angle X-ray diffraction (XRD) patterns of powder samples were obtained at room temperature by a Cu K α radiation ($\lambda = 1.788965 \text{ \AA}$) and using a D8 Advance X-ray diffractometer (Bruker, Germany). The supplied voltage and current were set to 40 kV and 120 mA. Samples were exposed at a scanning rate of $2\theta = 4^\circ \text{ min}^{-1}$ with 2θ values from 1.5° to 60° .

Thermogravimetric analysis (TGA) measurements were performed on a TGA/SDTA851e/SF/100 instrument. All samples were dried in a vacuum oven at 60°C prior to each TGA measurement to remove most of the water or volatile solvent. Samples weighing between 5 and 10 mg were heated from 20 to 850°C at a heating rate of $10^\circ \text{C min}^{-1}$ in nitrogen.

Magnetic studies were carried out with a MMVFTB Quantum Design SQUID magnetometer (Petersen Instruments Corporation) with fields up to 10 KOe at room temperature.

The UV-vis spectra and transmittance were recorded on an ultraviolet-visible spectrometer (UV/vis, Unico UV2102). The transmittance of the solution was measured at a wavelength of 485 nm using a thermostatically controlled cuvette.

Results and discussion

Preparation of polymer-modified superparamagnetic iron oxide nanoparticles and their characterization

Magnetic nanoparticles prepared by different synthetic methods may possess different properties, such as particle size, shape, magnetic properties, and so on. Sun *et al.*⁵⁰ proposed a high-temperature organic phase decomposition of an iron precursor method to synthesize iron oxide magnetic nanoparticles, which possess good crystallinity, and a relatively monodisperse and size-controlled distribution. Lattuada *et al.*²⁰ exploited the synthetic method to prepare OA/OAm-coated iron oxide magnetic nanoparticles using 1,2-tetradecane diol instead of the much more expensive 1,2-hexadecane diol. In the procedure, the heating stage was adjusted to control the average size and size distribution of nanoparticles. In our work, a similar procedure was adopted to prepare iron oxide magnetic nanoparticles, in the absence of expensive 1,2-hexadecane diol and 1,2-tetradecane diol, and the reaction mixture was first heated from room temperature to 100°C at the slow heating rate of $2^\circ \text{C min}^{-1}$. TEM and X-ray diffraction measurements were employed to characterize the structures of the synthetic iron oxide nanoparticles. TEM images of these nanoparticles are shown in Fig. 1. It can be seen from Fig. 1A that nanoparticles are roughly spherical or ellipsoidal shapes with a particle size of about 10 nm. Fig. 1B is the high-resolution TEM image, in which the lattice corresponds to a group of atomic plane fringes, indicating that the synthetic nanoparticles possess a good crystalline structure. Fig. 2A shows the XRD pattern of the synthetic iron oxide nanoparticles, in which six characteristic diffraction peaks for Fe_3O_4 ($2\theta = 30.2^\circ, 35.5^\circ, 43.6^\circ, 53.6^\circ, 57.3^\circ, 63.1^\circ$),^{17,50} marked by their indices ((220), (311), (400), (422), (511), (440)) can be observed. These results reveal that Fe_3O_4 nanoparticles can be prepared using the modified synthetic method. The sizes and size distributions of the freshly prepared Fe_3O_4 nanoparticles, $\text{Fe}_3\text{O}_4\text{-ol}$, can be also obtained by DLS measurement. DLS measurement of the freshly prepared Fe_3O_4 nanoparticles diluted in hexane provided an average hydrodynamic diameter of $\sim 17 \text{ nm}$

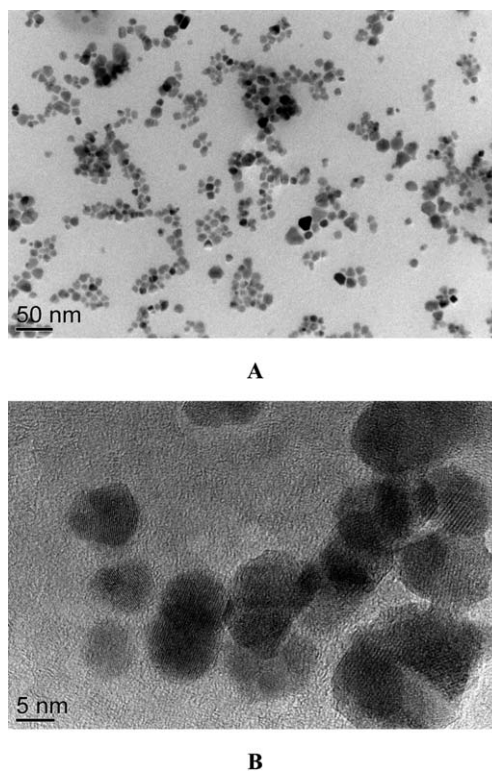


Fig. 1 TEM image (A) and high resolution TEM image (B) of $\text{Fe}_3\text{O}_4\text{-ol}$ nanoparticles.

and polydispersity indexes (PDI) of 0.116 (Fig. 3a). The difference from the particle sizes confirmed by TEM and DLS measurements was owing to the thicknesses of the OA/OAm layers on the nanoparticles surfaces.²⁰ The OA/OAm layers on the Fe_3O_4 nanoparticles can be proved by FT-IR measurement. The characteristic absorption bands at 2927 and 2856 cm^{-1} for methine groups originating from OA/OAm molecules, and the symmetric COO^- stretch peak at 1406 cm^{-1} can be observed in the FT-IR spectrum (Fig. 4a) of the synthetic Fe_3O_4 nanoparticle.²¹ On the other hand, the $\text{C}=\text{O}$ absorption peak at 1700 cm^{-1} of the oleic acid cannot be observed in the FT-IR spectrum of the freshly prepared Fe_3O_4 nanoparticles. The bonding of the

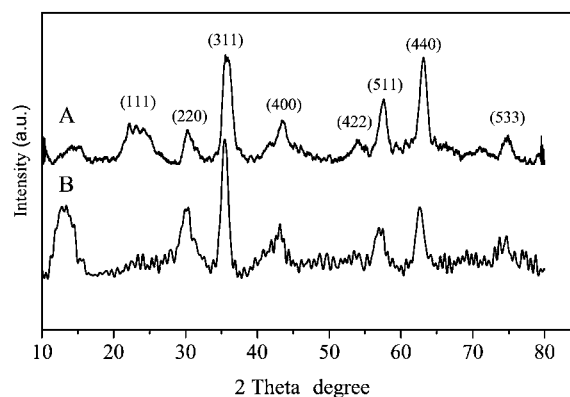


Fig. 2 XRD patterns of (A) $\text{Fe}_3\text{O}_4\text{-ol}$ and (B) $\text{Fe}_3\text{O}_4\text{-D}_{2.0}\text{-b-PDMAEMA-b-PNIPAM}$ cross-linked.

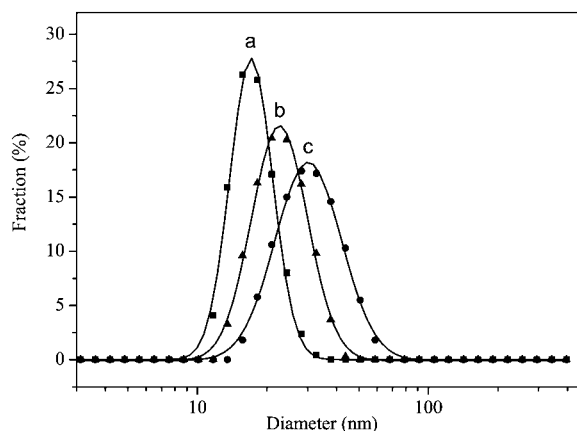


Fig. 3 DLS curves of (a) Fe_3O_4 -ol in hexane, (b) Fe_3O_4 - $\text{D}_{2.0}$ - b -PDMAEMA-Br in water and (c) cross-linking Fe_3O_4 - $\text{D}_{2.0}$ - b -PDMAEMA- b -PNIPAM in water.

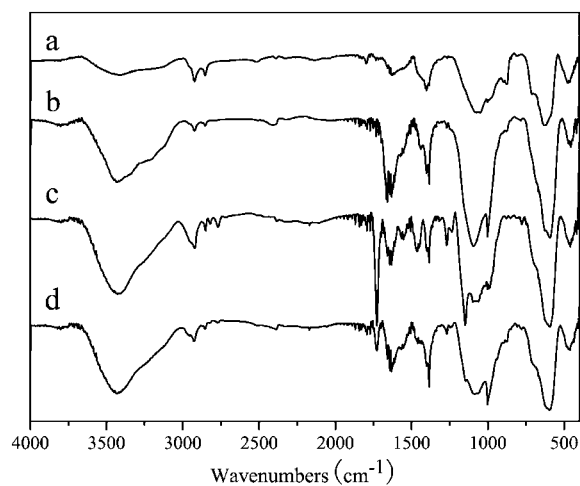


Fig. 4 FT-IR spectra of (a) Fe_3O_4 -ol, (b) Fe_3O_4 - $\text{D}_{2.0}$ -propargyl, (c) Fe_3O_4 - $\text{D}_{2.0}$ - b -PDMAEMA-Br and (d) Fe_3O_4 - $\text{D}_{2.0}$ - b -PDMAEMA- b -PNIPAM.

OA/OAm to Fe_3O_4 nanoparticle surfaces can certainly be claimed. Thermogravimetry (TG) measurements were also carried out to verify the bonding of the OA/OAm to Fe_3O_4 nanoparticle surfaces. As shown in Fig. 5a, the absolute mass loss of freshly prepared Fe_3O_4 nanoparticles, Fe_3O_4 -ol, is about 21% over the temperature range from room temperature to 850 °C.

The freshly prepared Fe_3O_4 nanoparticles can stably disperse in organic solvents such as toluene and hexane (see ESI, Figure S1:A†).^{20,50} To obtain water-soluble magnetic nanoparticles and improve their stability, hydrophilic polymers are introduced onto the magnetic nanoparticle surfaces by “grafting onto” and “grafting from” methods.^{1,3} In this contribution, the propargyl- $\text{D}_{2.0}$ -COOH dendron carrying four carboxyl groups was firstly chosen as a ligand to displace oleic acid from the Fe_3O_4 nanoparticle surfaces by the “grafting onto” method. It should be noted that the molecules bearing multiple carboxyl groups possess stronger binding capabilities and can be adsorbed more efficiently onto the iron oxide nanoparticle surfaces.²⁰ After modifying the OA/OAm-coated nanoparticles with propargyl- $\text{D}_{2.0}$ -COOH dendron, the characteristic absorption bands at

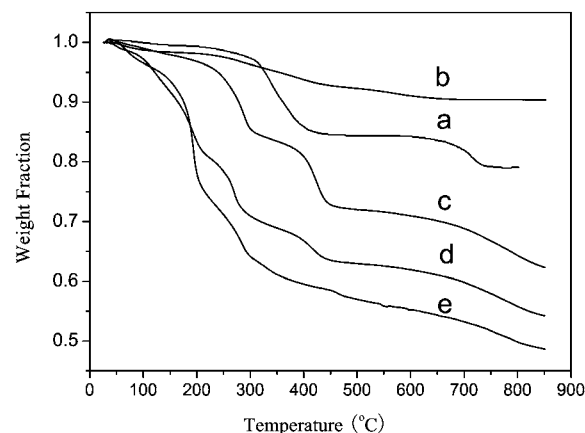


Fig. 5 TGA curves of (a) Fe_3O_4 -ol, (b) Fe_3O_4 - $\text{D}_{2.0}$ -propargyl, (c) Fe_3O_4 - $\text{D}_{2.0}$ - b -PDMAEMA-Br, (d) Fe_3O_4 - $\text{D}_{2.0}$ - b -PDMAEMA- b -PNIPAM and (e) Fe_3O_4 - $\text{D}_{2.0}$ - b -PDMAEMA- b -PNIPAM cross-linked.

1622 and 1550 cm^{-1} attributed to the acid amides stretch ($\delta_{\text{N-H}}$) of propargyl- $\text{D}_{2.0}$ appear in the FT-IR spectrum of propargyl- $\text{D}_{2.0}$ -modified Fe_3O_4 nanoparticles, Fe_3O_4 - $\text{D}_{2.0}$ -propargyl, as shown in Fig. 4b. The TGA profile of Fe_3O_4 - $\text{D}_{2.0}$ -propargyl shows a weight loss of about 10% over the entire temperature range and a slow rate of weight loss (Fig. 5b) between 300 °C and 650 °C compared with that of Fe_3O_4 -ol. Moreover, no weight losses are observed above 650 °C, which is obviously different from the TGA profile of Fe_3O_4 -ol.

On the other hand, the functional propargyl groups were also introduced onto the nanoparticle surfaces because of coating propargyl- $\text{D}_{2.0}$ -COOH dendrons, which was helpful to further modify the nanoparticles. To date, different controlled radical polymerization techniques have been utilized to modify the nanoparticle surfaces. Among these techniques, atom transfer radical polymerization (ATRP) has been most extensively used to modify the nanoparticles.^{17,39,43,51–53} Herein, the surface-initiated ATRP macroinitiator was prepared by Fe_3O_4 - $\text{D}_{2.0}$ -propargyl reacted with AEBIB by click chemistry. The sequential two steps of copper-mediated ATRP were used to polymerize monomers DMAEMA and NIPAM to the nanoparticle surfaces (see Scheme 1). After the first step of copper-mediated ATRP, $\text{D}_{2.0}$ - b -PDMAEMA-modified Fe_3O_4 nanoparticles (Fe_3O_4 - $\text{D}_{2.0}$ - b -PDMAEMA-Br) were obtained. From the FT-IR spectrum (Fig. 4c) of the purified Fe_3O_4 - $\text{D}_{2.0}$ - b -PDMAEMA-Br, an intense adsorption peak at 1728 cm^{-1} corresponding to the ester group stretch is clearly observed. The absorption band provides strong evidence that PDMAEMA has been grown from the nanoparticle surfaces *via* ATRP. At the same time, it demonstrated that the macroinitiator was successfully prepared by click chemistry. Compared with that of Fe_3O_4 - $\text{D}_{2.0}$ -propargyl (Fig. 5a), the TGA curve of PDMAEMA-modified nanoparticles (Fig. 5c) shows obviously a two-stage weight loss upon the heating process in nitrogen. A weight loss of about 14% is completed at 350 °C at the first stage, which is close to the weight loss of Fe_3O_4 - $\text{D}_{2.0}$ -propargyl and may be assigned to the $\text{D}_{2.0}$ -propargyl dendron degradation. The second stage accounts for about another 22% of the weight loss at the range of 380–850 °C, indicating the contribution of PDMAEMA. The DLS measurement of freshly PDMAEMA-modified nanoparticles diluted in

water provided an average hydrodynamic diameter of particles in solution equal to ~ 23 nm (Fig. 3b). The number-average molecular weight (M_n) and polydispersity index (PDI) of the grafted copolymers, $D_{2.0}$ -*b*-PDMAEMA-Br, obtained from Fe_3O_4 - $D_{2.0}$ -*b*-PDMAEMA-Br nanoparticles through the removal of Fe_3O_4 cores, were 4800 g mol^{-1} and 1.23 (see ESI, Figure S2†), respectively. The relatively narrow PDI indicated that the molecular weight of the grafted PDMAEMA on the surfaces of magnetic nanoparticles can be controlled by the ATRP approach. The chemical structures of $D_{2.0}$ -*b*-PDMAEMA-Br were further characterized by 1H NMR (see ESI†). The characteristic peaks of $D_{2.0}$ -*b*-PDMAEMA-Br macromolecules such as those of methylene ($-CH_2-$) originating from PDMAEMA block and methylene ($-CH_2-$) originating from $D_{2.0}$ block clearly appeared in the spectrum (see ESI, Figure S3†) at 4.35 and 3.55–3.49 ppm, respectively.

The prepared Fe_3O_4 - $D_{2.0}$ -*b*-PDMAEMA-Br was used as the macroinitiator to initiate monomer NIPAM polymerization for the preparation of $D_{2.0}$ -*b*-PDMAEMA-*b*-PNIPAM-modified nanoparticles, Fe_3O_4 - $D_{2.0}$ -*b*-PDMAEMA-*b*-PNIPAM, in the second step of copper-mediated ATRP. The peak at 1728 cm^{-1} (Fig. 4d) corresponding to the ester group stretch becomes weak, while the peaks at 1627 and 1556 cm^{-1} attributed to the amido bands of PNIPAM become stronger. As shown in Fig. 5d, a three-stage weight loss upon heating process can be clearly observed in the TGA curve of Fe_3O_4 - $D_{2.0}$ -*b*-PDMAEMA-*b*-PNIPAM. The weight losses of about 17%, 10% and 20%, which are sequentially completed at 235°C , 235 – 340°C , 340 – 850°C , can be clearly observed in the first, second and third stage, respectively. At the same time, it is estimated that the main contribution to the weight losses in the first, second and third stage should be originated from the degradation of the coated $D_{2.0}$ dendron, PDMAEMA and PNIPAM, respectively. After removal of Fe_3O_4 cores, M_n and PDI of the grafted copolymers $D_{2.0}$ -*b*-PDMAEMA-*b*-PNIPAM were 7400 g mol^{-1} and 1.17 (see ESI, Figure S2†), respectively. The increasing molecular weight and relatively narrow PDI indicated that the grafting PNIPAM process can be controlled by the ATRP approach. 1H NMR was further used to characterize the chemical structures of $D_{2.0}$ -*b*-PDMAEMA-*b*-PNIPAM (see ESI†). The inherent peaks of $D_{2.0}$ -*b*-PDMAEMA-*b*-PNIPAM macromolecules such as those of methylene ($-CH_2-$) assigned to PDMAEMA block, methylene ($-CH_2-$) originating from $D_{2.0}$ block and methyl (CH_3-) assigned to PNIPAM block clearly appeared in the spectrum (see ESI, Figure S3†) at 4.35, 3.55–3.49 and 1.05 ppm, respectively. The obtained results also indicated that $D_{2.0}$ -*b*-PDMAEMA-*b*-PNIPAM-modified nanoparticles were successfully prepared. On the other hand, according to the density of Fe_3O_4 , the diameter of the magnetic nanoparticles, and the weight losses and molecular weight obtained from the Fe_3O_4 - $D_{2.0}$ -*b*-PDMAEMA-Br and Fe_3O_4 - $D_{2.0}$ -*b*-PDMAEMA-*b*-PNIPAM nanoparticles, the graft density can be approximately 0.56 and 0.50 chains nm^{-2} , respectively (see ESI†). After surface-grafting with $D_{2.0}$ -*b*-PDMAEMA-*b*-PNIPAM, the magnetic nanoparticles can be dispersed in many organic solvents as well as water, such as ethanol, methanol, DMF and DMSO *etc.*

To further improve the stability of the block copolymer-modified nanoparticles, the cross-linking reaction between PDMAEMA chains and BIEE was carried out. Due to the cross-

linking reaction, a weight loss of about 52% can be observed in the TGA curve over the entire temperature range (Fig. 5e) and the behavior of thermal degradation is obviously different from that of Fe_3O_4 - $D_{2.0}$ -*b*-PDMAEMA-*b*-PNIPAM. After the cross-linking reaction, the magnetic nanoparticles can be stabilized in water, forming a stable brown solution and no precipitation occurs for 4 months (see ESI, Figure S1:C†). However, Fe_3O_4 - $D_{2.0}$ -*b*-PDMAEMA-*b*-PNIPAM nanoparticles can be only stabilized in water for 2 months (see ESI, Figure S1:B†). It is also verified that the cross-linking reaction can be helpful to stabilize magnetic iron oxide nanoparticles.⁴⁶ DLS measurements of freshly cross-linked block copolymer-modified nanoparticles diluted in water provided an average hydrodynamic diameter of particles in solution equal to ~ 32 nm (Fig. 3c). Its XRD pattern is shown in Fig. 2b. Compared with that of the OA/OAm-coated nanoparticles, the relative intensity and positions of the peaks were consistent. This revealed that the modification process did not result in the phase change of Fe_3O_4 .¹⁷

The magnetization curves measured at room temperature for the OA/OAm-coated Fe_3O_4 nanoparticles and the polymer-modified Fe_3O_4 nanoparticles are shown in Fig. 6. For the OA/OAm-coated Fe_3O_4 nanoparticles, after subtracting the organic layer weights based on the TGA result, the normalized saturation magnetization was 61.1 emu g^{-1} , which was lower than the bulk magnetic value of 90 emu g^{-1} .⁵⁴ This reduction in magnetization may be the result of noncollinear spins at the nanoparticle surface. At the same time, the saturation magnetizations for Fe_3O_4 - $D_{2.0}$ -*b*-PDMAEMA, Fe_3O_4 - $D_{2.0}$ -*b*-PDMAEMA-*b*-PNIPAM, and cross-linking Fe_3O_4 - $D_{2.0}$ -*b*-PDMAEMA-*b*-PNIPAM nanoparticles were normalized to 61.0, 41.5 and 17.7 emu g^{-1} based on subtracting the organic layer weights from the TGA results, respectively. The saturation magnetizations decreased with the increase of the organic layer thicknesses. On the other hand, it should be noted that no hysteresis curves can be observed in all samples, indicating the characteristic superparamagnetic behavior of all magnetic nanoparticles under room temperature (Fig. 6). These magnetic properties of polymer-modified nanoparticles also indicate that they are capable of

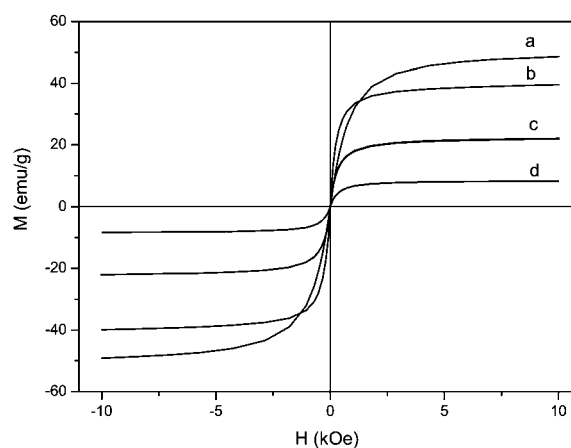


Fig. 6 Field dependent magnetization at room temperature for (a) Fe_3O_4 -ol, (b) Fe_3O_4 - $D_{2.0}$ -*b*-PDMAEMA-Br, (c) Fe_3O_4 - $D_{2.0}$ -*b*-PDMAEMA-*b*-PNIPAM and (d) Fe_3O_4 - $D_{2.0}$ -*b*-PDMAEMA-*b*-PNIPAM cross-linked.

responding to an external magnetic field and will show high trapping efficiency for magnetic targeting. To the best of our knowledge, it is first report for the synthesis of dendritic-linear block copolymer-modified magnetic nanoparticles.

In vitro thermosensitive drug release behaviors and anticancer activity assay

SPIONs have been utilized as a carrier for targeted drug delivery through the EPR effect⁵⁵ or by applying an external magnetic field.⁵⁶ Drug molecules were either entrapped in the SPION surface polymer layer through physical interactions (electrostatic, hydrophobic interaction, *etc*) or covalently conjugated to the functional groups on the SPION surface. DOX, as an anticancer drug model, has been extensively explored in the SPIONs system.^{2,57-61} In the contribution, to evaluate the block copolymer-modified Fe₃O₄ nanoparticles potential as a drug carrier, DOX was entrapped into D_{2.0}-*b*-PDMAEMA-*b*-PNIPAM-modified nanoparticles and cross-linking D_{2.0}-*b*-PDMAEMA-*b*-PNIPAM-modified nanoparticles, and the DOX release test in pH 7.4 PBS buffer solutions was performed at 25 °C and 37 °C. After removal of the free DOX, the drug loading efficiency of the block copolymer-modified nanoparticle was 22.7%. The DOX cumulative release results are shown in Fig. 7. In buffer solution at pH 7.4 in 5 h, the cumulative release amounts of DOX from uncross-linking block copolymer-modified nanoparticles were 28.8% and 15.5% at 25 °C and 37 °C, respectively, and those from cross-linking block copolymer-modified nanoparticles were 26.8% and 13.7% at 25 °C and 37 °C, respectively. This indicates that both uncross-linking and cross-linking polymer modified nanoparticles possess thermosensitive drug release behaviors, and the cumulative release amount was higher at 25 °C than at 37 °C. It can be explained that PNIPAM block chains are in the collapsed and hydrophobic conformation at 37 °C above the LCST,⁴⁷ which can retard drug release. This phenomenon can also be observed after 24 h (Fig. 7). On the other hand, the cumulative release amounts of DOX at 25 °C for uncross-linking block copolymer-modified nanoparticles increased from 28.8% to 55.0% with the change in cumulative release times from 5 h to 24 h. At the same conditions, the cumulative release amounts of

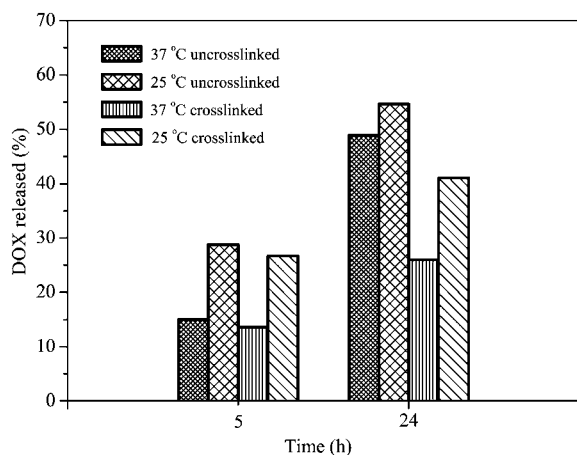


Fig. 7 Drug release profiles from DOX-loaded block copolymer-modified Fe₃O₄ nanoparticles.

DOX for cross-linking block copolymer-modified nanoparticles only increased from 26.8% to 41.1%. This indicates that the cross-linking structures retard drug release.

To assess the drug delivery potential of the DOX-loaded nanoparticles and the anticancer activity of the released DOX, *in vitro* cytotoxicity assays were performed by MTT assay against a HeLa cell line at different administered concentration of DOX ranging from 0.1 to 2 µg mL⁻¹. To compare the cytotoxic activity of the DOX-loaded nanoparticle with that of the free drug, the free DOX was used as a control. The HeLa cells proliferation results are shown in Fig. 8. It is found that the free DOX exhibits higher inhibition on HeLa cells in 24 h compared with the loaded DOX at the same DOX concentration when it is more than about 0.6 µg mL⁻¹. The doses required for 50% cellular growth inhibition (IC₅₀) of the DOX loaded in the modified nanoparticles with uncross-linking and cross-linking are 1.0 and 1.49 µg mL⁻¹, respectively, which are higher than the IC₅₀ of the free DOX (~0.66 µg mL⁻¹). The results are most likely related to the slow release of the drug from the drug-loaded nanoparticles in the course of incubation. In addition, the same antiproliferation effect on HeLa cells in 24 h requires higher concentration of DOX in the cross-linking block copolymer-modified nanoparticles than in the uncross-linking ones. This proves that the cross-linking structures can delay drug release. A possible reason is that more compact structures result in a lower diffusion rate of drug molecules after cross-linking. At the same time, the results verify that the encapsulation of DOX in the block copolymer-modified nanoparticles retards the toxic effect of DOX on the cells.⁵⁷ As a drug delivery system, the DOX-loaded nanoparticles are beneficial to decrease the side effects of DOX on cells.

Conclusions

The modified high-temperature solution phase reaction has been successfully used to prepare relatively monodisperse, superparamagnetic magnetite nanoparticles with a diameter size of about 10 nm. The propargyl focal point PAMAM-type dendrons with four carboxyl acid end groups as a cap displace the oleic acid and oleylamine on the magnetite nanoparticle surfaces by the “grafted onto” method. An initiator for ATRP was

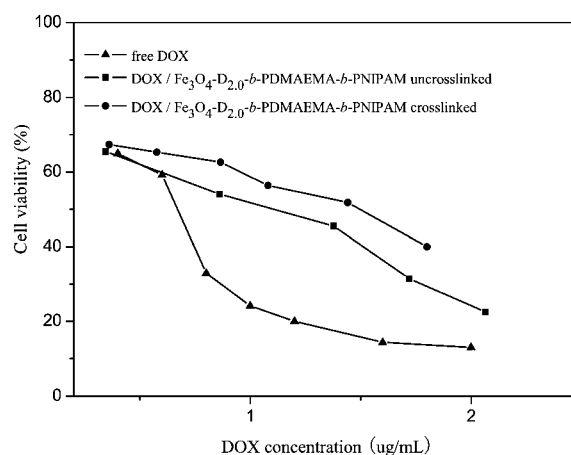


Fig. 8 Activity of DOX-loaded block copolymer-modified Fe₃O₄ nanoparticles against HeLa cells.

successfully introduced onto the surfaces of Fe₃O₄-D_{2.0}-propargyl *via* click chemistry. PDMAEMA and PNIPAM were grown gradually from nanoparticle surface using two-step copper-mediated ATRP. The block copolymer-modified magnetite nanoparticles can be stabilized in many organic solvents as well as water. The cross-linking reaction between PDMAEMA block with BIEE was obviously beneficial to increase the stability in water. In addition, doxorubicin (DOX) as anticancer drug model was loaded into the PAMAM-*b*-PDMAEMA-*b*-PNIPAM shell of the modified nanoparticles, and subsequently the drug release was performed in buffer solution (pH 7.4) at 25 °C or 37 °C. The results verify that block copolymer-modified nanoparticles as a drug carrier show thermosensitive drug release behaviors. Furthermore, MTT assay of DOX-loaded block copolymer-modified nanoparticles against Hela cells further confirm that the block copolymer-modified nanoparticles can be used for drug delivery. In a word, this approach represents a new strategy to prepare block copolymer-modified SPIONs that form greater stability in water, and further facilitate the potential biomedical applications of magnetic nanoparticles.

Acknowledgements

This work was financially supported by Shanghai Natural Scientific Foundation of China (10ZR1409500). Support from the Scientific Research Foundation for the Returned Overseas Chinese Scholars, State Education Ministry, and the financial support of the Shanghai Key Laboratory of Advanced Polymer Materials (ZD20100101), and Open Foundation of East China Normal University (ECNU2001-49) are also appreciated.

References

- 1 S. Laurent, D. Forge, M. Port, A. Roch, C. Robic, L. Vander Elst and R. N. Muller, *Chem. Rev.*, 2008, **108**, 2064–2110.
- 2 J. Kim, J. E. Lee, S. H. Lee, J. H. Yu, J. H. Lee, T. G. Park and T. Hyeon, *Adv. Mater.*, 2008, **20**, 478–483.
- 3 M. A. M. Gijs, F. D. R. Lacharme and U. Lehmann, *Chem. Rev.*, 2010, **110**, 1518–1563.
- 4 N. A. Frey, S. Peng, K. Cheng and S. Sun, *Chem. Soc. Rev.*, 2009, **38**, 2532–2542.
- 5 M. Mahmoudi, H. Hosseinkhani, M. Hosseinkhani, S. Boutry, A. Simchi, W. S. Journeay, K. Subramani and S. Laurent, *Chem. Rev.*, 2011, **111**, 253–280.
- 6 A. K. Gupta and M. Gupta, *Biomaterials*, 2005, **26**, 3995–4021.
- 7 C. Fang and M. Zhang, *J. Mater. Chem.*, 2009, **19**, 6258–6266.
- 8 J. Liu, S. Z. Qiao, Q. H. Hu and G. Q. Lu, *Small*, 2011, **7**, 425–443.
- 9 J. Gao, H. Gu and B. Xu, *Acc. Chem. Res.*, 2009, **42**, 1097–1107.
- 10 G. Huang, C. Zhang, S. Li, C. Khemtong, S.-G. Yang, R. Tian, J. D. Minna, K. C. Brown and J. Gao, *J. Mater. Chem.*, 2009, **19**, 6367–6372.
- 11 J. Park, M. K. Yu, Y. Y. Jeong, J. W. Kim, K. Lee, V. N. Phan and S. Jon, *J. Mater. Chem.*, 2009, **19**, 6412–6417.
- 12 R. Qiao, C. Yang and M. Gao, *J. Mater. Chem.*, 2009, **19**, 6274–6293.
- 13 K. C. Barick, M. Aslam, Y.-P. Lin, D. Bahadur, P. V. Prasad and V. P. Dravid, *J. Mater. Chem.*, 2009, **19**, 7023–7029.
- 14 J. Dobson, *Drug Dev. Res.*, 2006, **67**, 55–60.
- 15 R. Abu-Reziq, H. Alper, D. Wang and M. L. Post, *J. Am. Chem. Soc.*, 2006, **128**, 5279–5282.
- 16 B. Pan, D. Cui, Y. Sheng, C. Ozkan, F. Gao, R. He, Q. Li, P. Xu and T. Huang, *Cancer Res.*, 2007, **67**, 8156–8163.
- 17 Q. Zhang, C. Wang, L. Qiao, H. Yan and K. Liu, *J. Mater. Chem.*, 2009, **19**, 8393–8402.
- 18 S. Santra, C. Kaittanis, J. Grimm and J. M. Perez, *Small*, 2009, **5**, 1862–1868.
- 19 L. P. Ramírez and K. Landfester, *Macromol. Chem. Phys.*, 2003, **204**, 22–31.
- 20 M. Lattuada and T. A. Hatton, *Langmuir*, 2007, **23**, 2158–2168.
- 21 F. Hu, K. G. Neoh, L. Cen and E.-T. Kang, *Biomacromolecules*, 2006, **7**, 809–816.
- 22 S. Sun and H. Zeng, *J. Am. Chem. Soc.*, 2002, **124**, 8204–8205.
- 23 M. F. Casula, P. Floris, C. Innocenti, A. Lascialfari, M. Marinone, M. Corti, R. A. Sperling, W. J. Parak and C. Sangregorio, *Chem. Mater.*, 2010, **22**, 1739–1748.
- 24 Y.-X. Wang, S. Hussain and G. Krestin, *Eur. Radiol.*, 2001, **11**, 2319–2331.
- 25 C. Xu, K. Xu, H. Gu, X. Zhong, Z. Guo, R. Zheng, X. Zhang and B. Xu, *J. Am. Chem. Soc.*, 2004, **126**, 3392–3393.
- 26 L. Wang, Z. Yang, J. Gao, K. Xu, H. Gu, B. Zhang, X. Zhang and B. Xu, *J. Am. Chem. Soc.*, 2006, **128**, 13358–13359.
- 27 C. Zhang, B. Wängler, B. Morgenstern, H. Zentgraf, M. Eisenhut, H. Untenecker, R. Krüger, R. Huss, C. Seliger, W. Semmler and F. Kiessling, *Langmuir*, 2007, **23**, 1427–1434.
- 28 J. Gao, W. Zhang, P. Huang, B. Zhang, X. Zhang and B. Xu, *J. Am. Chem. Soc.*, 2008, **130**, 3710–3711.
- 29 J. Kim, S. Park, J. E. Lee, S. M. Jin, J. H. Lee, I. S. Lee, I. Yang, J.-S. Kim, S. K. Kim, M.-H. Cho and T. Hyeon, *Angew. Chem., Int. Ed.*, 2006, **45**, 7754–7758.
- 30 E. Strable, J. W. M. Bulte, B. Moskowitz, K. Vivekanandan, M. Allen and T. Douglas, *Chem. Mater.*, 2001, **13**, 2201–2209.
- 31 C. R. Vestal and Z. J. Zhang, *J. Am. Chem. Soc.*, 2002, **124**, 14312–14313.
- 32 G. D. Moeser, W. H. Green, P. E. Laibinis, P. Linse and T. A. Hatton, *Langmuir*, 2004, **20**, 5223–5234.
- 33 A. Ditsch, P. E. Laibinis, D. I. C. Wang and T. A. Hatton, *Langmuir*, 2005, **21**, 6006–6018.
- 34 M. Lattuada and T. A. Hatton, *J. Am. Chem. Soc.*, 2007, **129**, 12878–12889.
- 35 H. He, Y. Zhang, C. Gao and J. Wu, *Chem. Commun.*, 2009, 1655–1657.
- 36 C. Liu, J. Guo, W. Yang, J. Hu, C. Wang and S. Fu, *J. Mater. Chem.*, 2009, **19**, 4764–4770.
- 37 S. Si, A. Kotal, T. K. Mandal, S. Giri, H. Nakamura and T. Kohara, *Chem. Mater.*, 2004, **16**, 3489–3496.
- 38 A. F. Thünemann, D. Schütt, L. Kaufner, U. Pison and H. Möhwald, *Langmuir*, 2006, **22**, 2351–2357.
- 39 P. L. Golas, S. Louie, G. V. Lowry, K. Matyjaszewski and R. D. Tilton, *Langmuir*, 2010, **26**, 16890–16900.
- 40 T. J. Daou, G. Pourroy, J. M. Greneche, A. Bertin, D. Felder-Flesch and S. Begin-Colin, *Dalton Trans.*, 2009, 4442–4449.
- 41 A. M. Schmidt, *Macromol. Rapid Commun.*, 2005, **26**, 93–97.
- 42 K. Matyjaszewski and J. Xia, *Chem. Rev.*, 2001, **101**, 2921–2990.
- 43 R. I. Barbey, L. Lavanant, D. Paripovic, N. Schüwer, C. Sugnaux, S. Tugulu and H.-A. Klok, *Chem. Rev.*, 2009, **109**, 5437–5527.
- 44 A. J. L. Villaraza, A. Bumb and M. W. Brechbiel, *Chem. Rev.*, 2010, **110**, 2921–2959.
- 45 D. Astruc, E. Boisselier and C. t. Ornelas, *Chem. Rev.*, 2010, **110**, 1857–1959.
- 46 Y. Chen, J. Cho, A. Young and T. A. Taton, *Langmuir*, 2007, **23**, 7491–7497.
- 47 H. Wei, S.-X. Cheng, X.-Z. Zhang and R.-X. Zhuo, *Prog. Polym. Sci.*, 2009, **34**, 893–910.
- 48 V. J. Gatto, K. A. Arnold, A. M. Viscariello, S. R. Miller, C. R. Morgan and G. W. Gokel, *J. Org. Chem.*, 1986, **51**, 5373–5384.
- 49 M. Ciampolini and N. Nardi, *Inorg. Chem.*, 1966, **5**, 41–44.
- 50 S. Sun, H. Zeng, D. B. Robinson, S. Raoux, P. M. Rice, S. X. Wang and G. Li, *J. Am. Chem. Soc.*, 2004, **126**, 273–279.
- 51 J. Pyun, T. Kowalewski and K. Matyjaszewski, *Macromol. Rapid Commun.*, 2003, **24**, 1043–1059.
- 52 S. Shylesh, V. Schünemann and W. R. Thiel, *Angew. Chem., Int. Ed.*, 2010, **49**, 3428–3459.
- 53 J. Zhou, L. Wang, J. Ma, J. Wang, H. Yu and A. Xiao, *Eur. Polym. J.*, 2010, **46**, 1288–1298.
- 54 V. T. Binh, S. T. Purcell, V. Semet and F. Feschet, *Appl. Surf. Sci.*, 1998, **130–132**, 803–814.
- 55 M. K. Yu, Y. Y. Jeong, J. Park, S. Park, J. W. Kim, J. J. Min, K. Kim and S. Jon, *Angew. Chem., Int. Ed.*, 2008, **47**, 5362–5365.
- 56 A. Kumar, P. K. Jena, S. Behera, R. F. Lockey, S. Mohapatra and S. Mohapatra, *Nanomed.: Nanotechnol., Biol. Med.*, 2010, **6**, 64–69.

-
- 57 S. R. Deka, A. Quarta, R. D. Corato, A. Riedinger, R. Cingolani and T. Pellegrino, *Nanoscale*, 2011, **3**, 619–629.
- 58 L. Guo, H. Ji, X. Zhang, Y. Li and L. Zheng, *J. Mater. Chem.*, 2008, **18**, 5993–5997.
- 59 E. Munnier, S. Cohen-Jonathan, C. Linassier, L. Douziech-Eyrolles, H. Marchais, M. Soucé, K. Hervé, P. Dubois and I. Chourpa, *Int. J. Pharm.*, 2008, **363**, 170–176.
- 60 J. H. Maeng, D.-H. Lee, K. H. Jung, Y.-H. Bae, I.-S. Park, S. Jeong, Y.-S. Jeon, C.-K. Shim, W. Kim, J. Kim, J. Lee, Y.-M. Lee, J.-H. Kim, W.-H. Kim and S.-S. Hong, *Biomaterials*, 2010, **31**, 4995–5006.
- 61 P. Zou, Y. Yu, Y. A. Wang, Y. Zhong, A. Welton, C. Galbán, S. Wang and D. Sun, *Mol. Pharmaceutics*, 2010, **7**, 1974–1984.